Nano Energy 112 (2023) 108509

Contents lists available at ScienceDirect

Nano Energy

journal homepage: www.elsevier.com/locate/nanoen

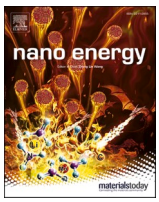

Full paper

Triboelectric-material-pairs selection for direct-current triboelectric nanogenerators☆

Shengnan Cui [a,1,1], Di Liu [a,b,1], Peiyuan Yang [a], Jiaqi Liu [a], Yikui Gao [a,b], Zhihao Zhao [a,b], Linglin Zhou [a,b], Jiayue Zhang [a,b,c], Zhong Lin Wang [a,b,c,*], Jie Wang [a,b,*]

[a] Beijing Institute of Nanoenergy and Nanosystems, Chinese Academy of Sciences, Beijing 101400, PR China
[b] College of Nanoscience and Technology, University of Chinese Academy of Sciences, Beijing 100049, PR China
[c] School of Materials Science and Engineering, Georgia Institute of Technology, Atlanta 30332, USA

ARTICLE INFO

Keywords:
Direct-current triboelectric nanogenerator
Triboelectric material pair
Electrostatic breakdown
Leakage current
Breakdown efficiency

ABSTRACT

Direct-current triboelectric nanogenerator (DC-TENG) arising from electrostatic breakdown exhibits unique merits over conventional alternating-current TENGs, such as the constant-current output and high output charge density. The selection of appropriate triboelectric material pair (TMP) is important for improving its performance. Here, we propose a universal strategy for the TMP selection of DC-TENG by simultaneously considering the friction, dielectric and triboelectric performance. Based on assessing five basic parameters in DC-TENG, including the friction coefficient, surface charge density, leakage current, breakdown charge density and breakdown efficiency, it is found that the thermoplastic urethanes (TPU)-ethylene-tetra-fluoro-ethylene (ETFE) pair presents considerable output performance. Finally, a micro-structured DC-TENG with a designed power-management circuit was fabricated to further demonstrate the enhanced performance of DC-TENG with TPU-ETFE as the TMP. This work provides an effective strategy to select appropriate TMPs to optimize the performance of DC-TENG, facilitating its practical applications.

1. Introduction

As the world enters the 5G technology era, the burgeoning distributed electronics and sensors are essential to acquire all kinds of information in the environment and to build the connection between human and things, which are also the basis for artificial intelligence (AI) and the internet of things (IoTs). To powering these numerously and randomly distributed electronic devices, it is commonly considered that only relying on the traditional "ordered" energy and batteries is not an ideal choice, and the "random" energy harvested from the environment provides an alternative solution. Various efforts have been devoted to developing the energy harvesting technologies, such as solar cells, thermoelectric nanogenerators, piezoelectric nanogenerators and triboelectric nanogenerators (TENGs), to convert various environmental energies into electricity providing energy supply for those electronics [1]. Among them, TENG, based on triboelectrification (TE) and electrostatic induction, has attracted vast research interest owing to its unique merits of light weight, low cost, broad material availability and excellent mechanical-electric energy conversion capability at low frequency, which undoubtedly provides a potential solution to power the widely distributed electronic devices and sensors [2–9].

Improving the charge density is essential to the optimization of TENG, because the power density is proportional to the square of charge density [10,11]. Although many approaches have been proposed to boost the charge density through ion injection [12], material selection [13], soft contact [14] and other methods in atmospheric environment, the surface charge density is still limited by the air breakdown effect. For instance, the charge density of TENG reaches 1003 μC m^{-2} in vacuum, while only 250 μC m^{-2} was obtained in atmosphere condition [15]. Moreover, the conventional TENG has the characteristics of alternating current (AC) and pulse output, which needs the rectifier to obtain direct-current (DC) output for powering electronics, inevitably leading

☆ "Prof Zhong Lin Wang, an author on this paper, is the Editor-in-Chief of Nano Energy, but he had no involvement in the peer review process used to assess this work submitted to Nano Energy. This paper was assessed, and the corresponding peer review managed by Professor Chenguo Hu, also an Associate Editor in Nano Energy"

* Corresponding authors at: Beijing Institute of Nanoenergy and Nanosystems, Chinese Academy of Sciences, Beijing 101400, PR China.
E-mail addresses: zhong.wang@mse.gatech.edu (Z.L. Wang), wangjie@binn.cas.cn (J. Wang).

[1] These authors contributed equally.

https://doi.org/10.1016/j.nanoen.2023.108509
Received 10 March 2023; Received in revised form 19 April 2023; Accepted 5 May 2023
Available online 7 May 2023

to energy loss. In recent years, the direct-current TENG (DC-TENG) based on TE and electrostatic breakdown has been developed and provides a feasible solution to simultaneously solve the above issues, which even shows superior advantages over the conventional TENGs, such as the DC or even constant current output, high output charge density and power density, and anti-electromagnetic interference for sensing [16,17]. The charge density enhancement of DC-TENG is of great significance for quadratically increase its power density and linearly increase its sensor sensitivity, whose restricted factors can be expressed by the following equation[18]:

$$\sigma_{DC-TENG} = k \times \min(\sigma_{triboelectrification}, \sigma_{c,electrostatic\quad breakdown}) \tag{1}$$

where $\sigma_{triboelectrification}$ is the triboelectric charge density, $\sigma_{c,\ electrostatic\ breakdown}$ is the charge density in the electrostatic breakdown process and k is the electrode structure factor. Several approaches have been proposed to increase the $\sigma_{triboelectrification}$ including the interface liquid lubrication[19] and material selection [20]; increase the $\sigma_{c,\ electrostatic\ breakdown}$ such as high temperature, appropriate low pressure [21], atmospheric control and field enhancement [22,23]; increase k value by rational structural design [18,24]. Nevertheless, $\sigma_{triboelectrification}$ is the basic electric parameter related to the triboelectric material pair (TMP) during the TE process, and determines the output performance of DC-TENGs. In this context, selecting appropriate TMPs is one of the effective and simple directions to optimize the performance of

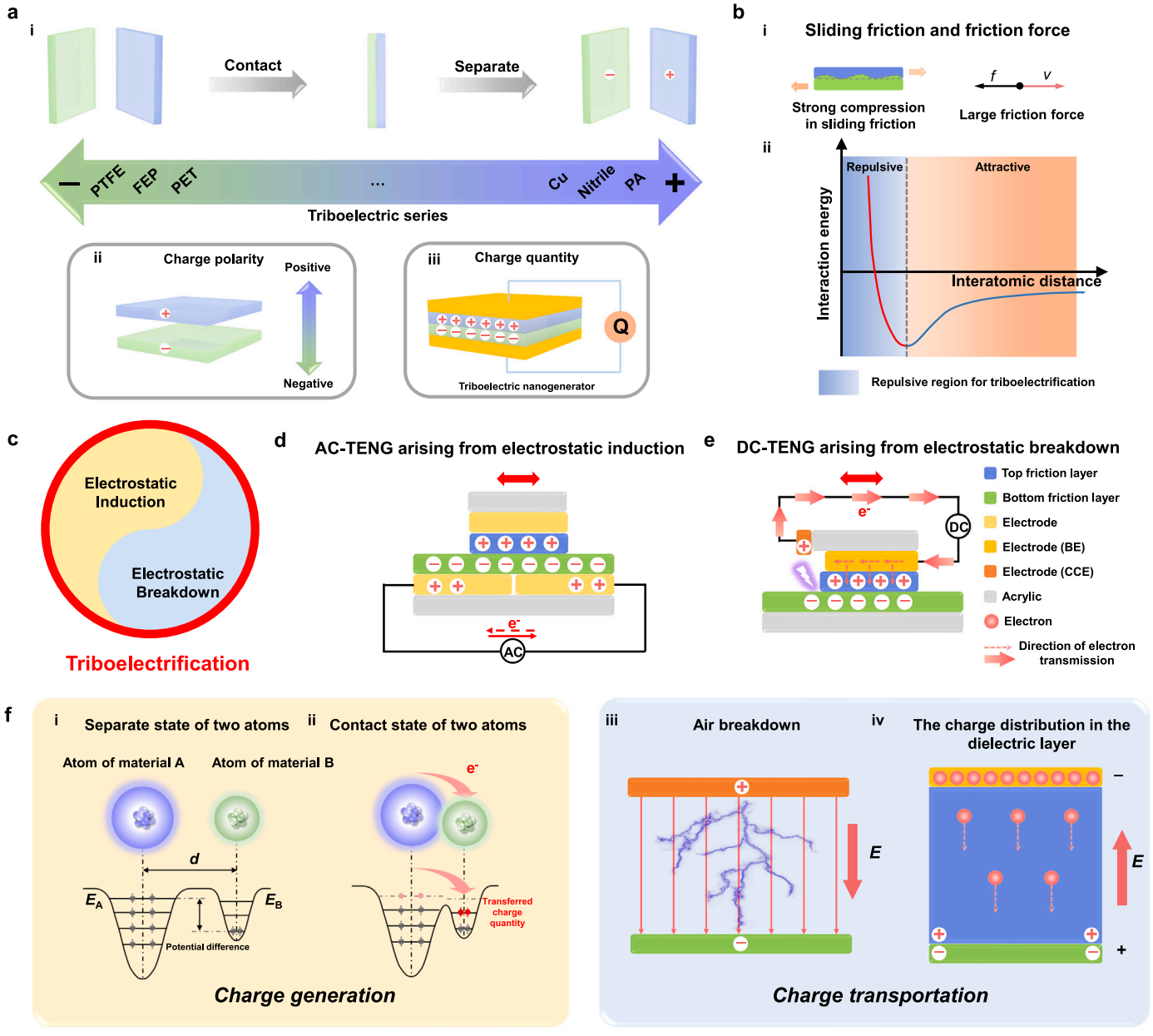

Fig. 1. Triboelectrification and triboelectric nanogenerator. (a) Represented qualitative triboelectric series (i). The conventional triboelectric series is determined by charge polarity (ii), while the output performance of TENG is decided by the charge quantity (iii). (b) Sliding friction and friction force of triboelectric material pairs at repulsive region for triboelectrification. i: Sliding friction is usually accompanied by a large friction force. ii: The high triboelectrification occurs at repulsive region. (c) Triboelectrification can combine the electrostatic induction to form the AC-TENG or combine the electrostatic breakdown to form the DC-TENG. (d) The mechanism of AC-TENG. (e) The mechanism of DEDC-TENG. (f) The charge generation and charge transportation processes of DEDC-TENG. i: The electron cloud model of two atoms when the atoms of material A and material B are at the separate state. ii: The electron cloud model of two atoms when the atoms of material A and material B are at the contact state. iii: The air breakdown process in DEDC-TENG. iv: The charge distribution in the dielectric layer of DEDC-TENG. d, the distance between two atoms; E_A and E_B are the occupied energy levels of electrons.

DC-TENGs [20,25]. Specifically, many works have shown that the dielectric-dielectric layer TMP exhibits better TE performance than the metal-dielectric layer [26,27]. Recently, a dielectric enhancement effect was proposed to improve the output performance of the dielectric enhanced DC-TENG (DEDC-TENG) by selecting an appropriate dielectric pair with stronger TE as TMP[28]. However, the friction performance such as friction force should be considered in sliding motion, and the dielectric performance such as polarization and leakage current also are vital parameters influencing the performance of DC-TENGs [20,28]. Therefore, a guideline for the selection of appropriate TMP simultaneously considering the friction, dielectric and triboelectric properties is highly desired to optimize the performance of DEDC-TENG and promote its wide applications.

In this work, considering the friction, dielectric and triboelectric performance of TMPs, we put forward a universal strategy to assess whether a TMP is suitable for DEDC-TENG. We analyzed the charge generation and charge transportation processes in the DC-TENG based on its basic working mechanism, and it is found that the five indicators, including the friction coefficient, surface charge density, leakage current, breakdown charge density and breakdown efficiency, can be considered as the basic parameters to select appropriate TMPs for DEDC-TENG. Based on the five indicators, the TPU-ETFE pair presents excellent comprehensive output performance for DEDC-TENG. Specifically, the micro-structured DC-TENG with four units can be used for powering 40 LEDs or a hygrothermograph at the low working frequency of 0.85 Hz with a designed power-management circuit. This work provides a universal strategy for the selection of suitable TMPs in DC-TENG, and highlights regulating the charge generation and transportation processes in TENG to optimize its performance.

2. Results

2.1. Triboelectrification and triboelectric nanogenerator

Contact electrification is the electrification effect caused by contact or friction of two different materials, in which a material carries net positive charges while the other carries net negative charges. Generally, the triboelectric performance of different materials can be evaluated by the triboelectric series, which ranks the material by the tendency to gain or get electrons playing an important role for applications of contact electrification (Fig. 1a). Among the numerous applications of contact electrification, TENG has attracted much interest in recent years for its extensive application in energy harvesting and self-powered sensor fields. Obviously, the conventional triboelectric series provides a certain reference value to select suitable TMPs for TENGs. However, it only represents the relative charge polarity of the TMPs rather than charge quantities, while the output performance of TENG relies on not only the charge polarity but also the quantity of transferred charge. In other words, to select appropriate TMPs for TENGs, both the charge polarity and quantity should be considered.

Comparing with the contact-separating electrification, the sliding electrification has a higher charge generation efficiency, which has been widely used for building high-performance TENGs, especially for the sliding mode DC-TENG [9]. It is noteworthy that a strong compression is inevitable in sliding electrification, which generally results in a large friction force (Fig. 1b). From the interatomic interaction potential, the high TE occurs at the repulsive region where the electron cloud overlapped under the strong pressure, which further leads to large friction force. Therefore, an appropriate friction coefficient (μ) of TMP is essential and should be carefully investigated first in DC-TENG.

From the basic working mechanism of TENG, the charges generated by TE can combine the electrostatic induction to form the AC-TENG or combine the electrostatic breakdown to form the DC-TENG (Fig. 1c). The AC-TENG such as freestanding mode TENG can be used as a tool to investigate the TE performance of TMPs (Fig. 1d). For the DEDC-TENG here, the output arises from the combination of TE derived from TMP, electrostatic breakdown in the air gap and leakage current through the top dielectric layer (Fig. 1e). The dielectric and triboelectric performance of TMP is closely related to the charge generation and charge transportation processes. The charge generation process can be obtained from the electron cloud model depicted in Fig. 1f [29–31]. When the atoms of material A and material B are at the separate state, the electrons are trapped in a particular orbit by the potential well and without the ability to move freely (Fig. 1f i). Once the two atoms contact with each other under the applied force, the electron cloud will overlap and form bond, and the electrons can transfer at the reduced energy barrier (Fig. 1f ii). The electron cloud varies from materials, so the transferred charge quantity generated by TE relies on the materials' properties in specific TMPs. The charge transportation process in DEDC-TENG mainly contains the charge flow by air breakdown and leakage current (Note S1). The surface charges on the bottom friction layer transfer to the charge collecting electrode (CCE) based on air breakdown. It is noted that the electric field near the surface of bottom friction layer may cause the internal polarization of bottom friction layer, reducing the electric field across the air gap and decreasing the output, so the polarization intensity of the bottom friction layer is an important parameter for DEDC-TENG (Fig. 1f iii). Once the breakdown charges reach the back electrode (BE) from the external circuit, the charges should be permitted to pass through the top friction layer in the form of leakage current, so the leakage current of the top friction layer also is an essential parameter for DEDC-TENG (Fig. 1f iv). Overall, considering the charge generation and charge transportation processes in the DEDC-TENG, we preliminarily consider that the friction coefficient, surface charge, polarization intensity and leakage current are the key factors to select the appropriate TMPs for DEDC-TENG.

2.2. Friction behavior and triboelectric performance of various TMPs

To investigate the influence of friction behavior and electrical properties of TMPs on DC-TENG, we measure the μ and triboelectric charge of TMPs. It is obviously that μ is the primary crucial parameter for the selection of TMPs. Only possessing a low μ can ensure a small friction resistance to reduce energy loss. Here, thermoplastic urethanes (TPU), Polyamide (PA) and Nitrile, which are easy to lose electrons, are selected as top friction layers; Ethylene-Tetra-Fluoro-Ethylene (ETFE), Polytetrafluoroethylene (PTFE), Polyfluoroalkoxy (PFA), Fluorinated ethylene propylene (FEP), Polyvinyl chloride (PVC), Polyethylene terephthalate (PET) and Polycarbonate (PC), which are considered as representative materials to gain electrons in TENGs, are selected as bottom friction layers. In addition, the copper was selected to construct the metal-dielectric TMP as a reference for comparison. The μ of the TMPs are tested as Fig. 2a and the measuring equipment is shown in Fig. S1 and Note S2. The dielectric-dielectric pair with the highest friction coefficient is PA-PC of 1.97 and the lowest is TPU-PTFE of 0.21. To keep a relatively smooth sliding process and reduce wear, TMPs of Nitrile-ETFE, TPU-PVC, PA-PVC, Nitrile-PVC, Nitrile-PET, PA-PC, Nitrile-PC with large value of μ ($\mu > 1$) were excluded.

The freestanding mode AC-TENG is used as a tool for measuring the triboelectric charge of TMPs, and its working mechanism is depicted in Fig. S2 and Note S3. The output charge of AC-TENG with different TMPs are depicted in Fig. 2b and the corresponding output current is shown in Fig. S3. It is obvious that the output charge of dielectric-dielectric layer is higher than that of corresponding Cu-dielectric layer for all TMPs, due to the higher TE performance of dielectric-dielectric pairs. Among the dielectric-dielectric TMPs, the transferred charges of TMP for TPU-ETFE, PA-ETFE, TPU-PTFE, PA-PTFE, Nitrile-PTFE, TPU-PFA, PA-PFA, Nitrile-PFA, TPU-FEP, PA-FEP present great performance. Specifically, the TPU-ETFE pair has the highest output charge being 241.6 nC. It is noted that the direction of charge transfer of TPU-PC is on the contrary with other TMP, which response the easier ability of losing electrons of PC than TPU. By selecting different TMPs, the process of charge generation can be regulated, and the triboelectric charge density can be optimized.

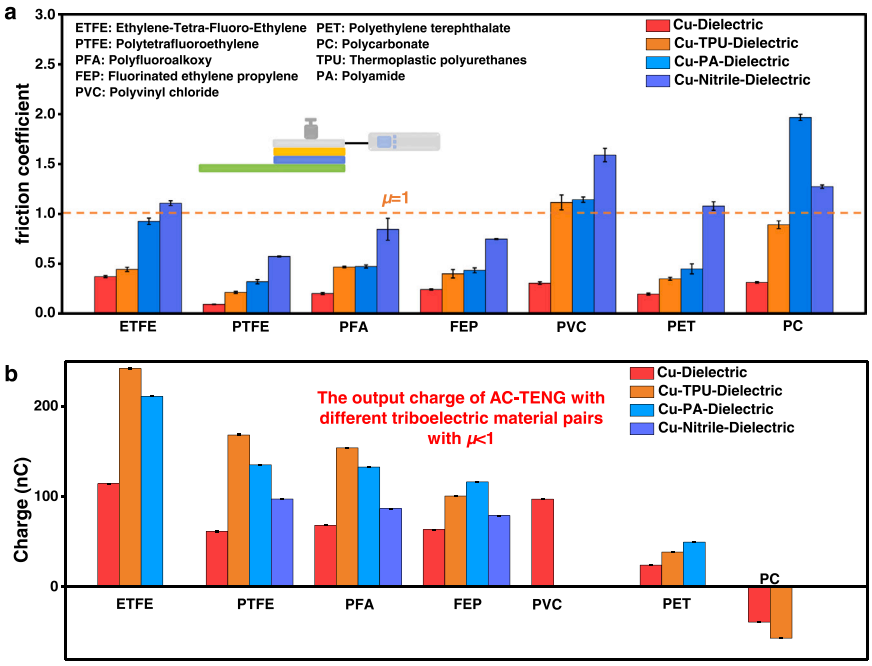

Fig. 2. Friction behavior and triboelectric performance of TENG with different triboelectric material pairs. (a) The Friction coefficient (μ) between various triboelectric material pairs. (b) The output charge of AC-TENG with different triboelectric material pairs, where the triboelectric material pairs with friction coefficient greater than 1 are excluded.

Furthermore, to investigate the effect of different thickness of bottom dielectric layer on TE performance, we take the TPU-FEP pair as an example and the results indicate that the thickness of FEP has little effect on the TE performance with certain range (Fig. S4).

2.3. Electric performance of DC-TENG with different TMPs

To investigate the electric performance of DC-TENG with different TMPs, we measure the corresponding parameters of materials which related to the charge generation and charge transportation processes of DC-TENG. Also, the copper was selected to construct the metal-dielectric TMP as a reference for comparison. The detailed working mechanism of DEDC-TENG is shown in Fig. 3a. At the initial state, the TMP contacts with each other and carries opposite charges due to the different ability of losing electrons (Fig. 3a, i). When the slider moves to right in horizontal direction and the CCE reaches the above of bottom dielectric layer, there will be a high electric field between the CCE and the bottom dielectric layer. Once the value of electric field exceeds approximate 3 kV mm^{-1}, the surrounding air will be ionized and the negative charges on the bottom dielectric transfer to the CCE. Then the charges flow from the CCE to the BE via the external circuit and pass through the top dielectric layer in the form of leakage current (Fig. 3a, ii). Therefore, $I_{leakage}$ is a crucial parameter for selecting the top dielectric layer. Through applying the bias voltage on the dielectric material with silver-sputtered on both sides, $I_{leakage}$ of different materials was tested based on the high precision insulation resistance meter (Fig. 3b). The $I_{leakage}$ of the conventional materials like ETFE, PTFE, PFA, FEP, PVC, PET and PC under a bias voltage of 100 V is less than 1 nA; the $I_{leakage}$ of TPU, PA, Nitrile is 0.53, 0.367, 4.52 μA respectively, which is suitable being the top dielectric layer. Besides, the $I_{leakage}$ of different dielectric materials under different bias voltage is presented in Fig. S5 and shows a rising trend with the increase of voltage.

The output charge of DC-TENG is presented in Fig. 3c, where the TMPs with μ greater than 1 also are excluded (Fig. S6). Taking DEDC-TENG employing TPU-FEP as TMP as an example, the output waveform is shown in Fig. S7. For all TMPs, the output of DC-TENG with the dielectric-dielectric layer is higher than that with the corresponding Cu-dielectric layer. The transferred charges of TMPs for TPU-ETFE, PA-ETFE, TPU-PTFE, PA-PTFE, Nitrile-PTFE, TPU-PFA, PA-PFA show great performance, and the TPU-ETFE pair has the highest output charge. The direction of charge transfer of TPU-PC is on the contrary with other TMPs, which again indicates that the ability of losing electrons of PC is stronger than TPU. According to the above results, the output charge density of DC-TENG is related to the triboelectric charge density of TMPs and their trends are almost consistent. The current of DC-TENG is depicted in Fig. 3d and Fig. S8, which almost maintain the same tendency with the transferred charges. Given that the electric filed in the bottom friction layer caused by TE may induce internal polarization and affect the process of air breakdown, the polarization vs. electric field loops for different dielectric films under various electric fields are depicted in Fig. S9. It exhibits that the dielectric material without significant polarizing effect nearly has no effect on the output charges in DC-TENG, while the dielectric material with strong polarizing effect decreasing the electric field across the air gap and then reduced the output charges in DC-TENG (Fig. S10 and Note S4). Moreover, the breakdown efficiency (η) of various TMPs in DEDC-TENG, which depicted as the ratio of output charge density to the triboelectric charge density, is shown in Fig. S11 and Note S5.

2.4. Comprehensive selection rules of triboelectric materials for DEDC-TENG

The parameters mentioned above are analyzed separately without systematically considering the complicated practical situation with corresponding requirement. It's essential to consider various parameters in a comprehensive way and analyze whether the TMP is suitable for DEDC-TENG to cope with various practical application scenarios. For instance, the output charge density of DC-TENG (σ_{DC}) and η are important factors for an energy harvesting device; in the condition of low driving mechanical force, a smaller μ is preferred. According to the above comparison, considering the friction force, triboelectric and dielectric performance of TMP, we establish a systematic radar chart to evaluate the performance of TMP as shown in Fig. 4. We take the surface charge density of AC-TENG (σ_{SC}), σ_{DC}, η, μ and $I_{leakage}$ into account, and

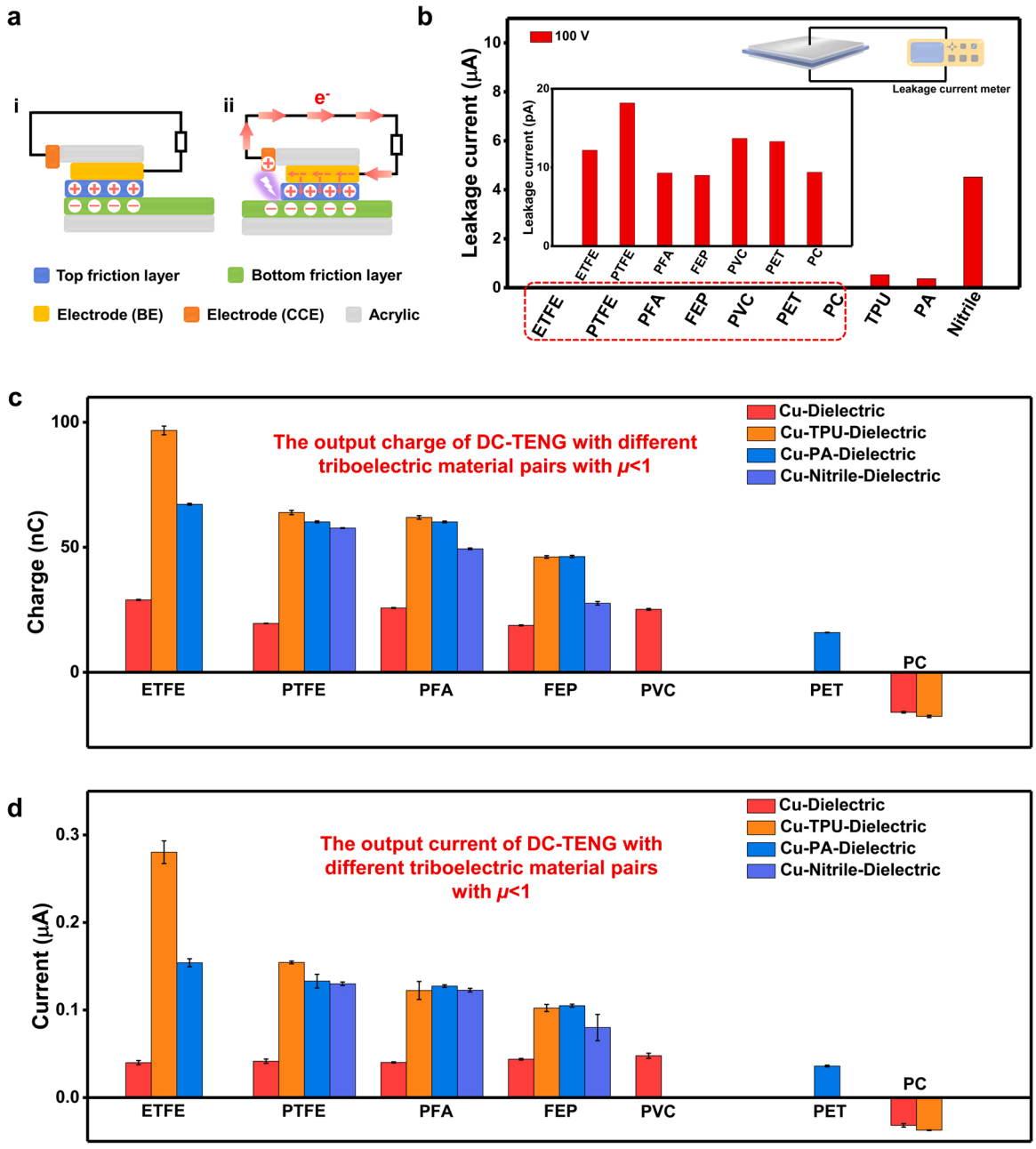

Fig. 3. Electric performance of DC-TENG with different triboelectric material pairs. (a) Working mechanism of DC-TENG with different triboelectric material pairs. (b) The leakage current of different dielectric films. (c) The output charge of DC-TENG with different triboelectric material pairs. (d) The output current of DC-TENG with different triboelectric material pairs.

σ_{SC}* , σ_{DC}* , η * , and $1/\mu$ * are the normalization of σ_{SC}, σ_{DC}, η and the reciprocal of the friction coefficient ($1/\mu$), and $I_{leakage}$* is depicted in Note S6. These values are detailly shown in Table S1. From the analysis of the charge generation and charge transportation processes, a suitable TMP for DEDC-TENG should possess the following characteristics: an appropriate friction coefficient to realize the easily sliding motion; the high triboelectric charge density to ensure high energy conversion efficiency from mechanical energy to electrostatic energy; a certain leakage current to build the circuit loop; a high breakdown efficiency to ensure high energy conversion efficiency from electrostatic energy to the final electric energy. As an energy conversion device, the primary factor should be considered is the output performance. We have analyzed and counted all the materials, among which TPU-ETFE, PA-ETFE, TPU-PTFE, PA-PTFE, Nitrile-PTFE, TPU-PFA, PA-PFA with high output performance is in the candidate list. Specifically, the PA-ETFE was excluded due to its large friction coefficient of 0.9 which is unapt to slide and has a low breakdown efficiency. The TPU-ETFE, TPU-PTFE, PA-PTFE, Nitrile-PTFE, TPU-PFA, PA-PFA are selected as the appropriate TMPs for designing DEDC-TENG. Comparing with the TPU-ETFE, TPU-PTFE and TPU-PFA, the PA-PTFE, Nitrile-PTFE and PA-PFA show relatively moderately comprehensive performance. The TPU-ETFE shows excellent σ_{SC}* and σ_{DC}* , and its η is approximately 0.3. Meantime, it has a proper friction performance, and its $1/\mu$ * reaches to 0.32. The TPU-PTFE has excellent friction performance, which $1/\mu$ * is up to 1, but its σ_{SC}* and σ_{DC}* are relatively low comparing with the TPU-ETFE.

Besides, as for durability, the TENG in sliding mode inevitably suffers from wear due to friction force, which is also an issue that limits further application of DEDC-TENG. However, the previous work came up with a feasible solution about adding lubricant during the operation[19],

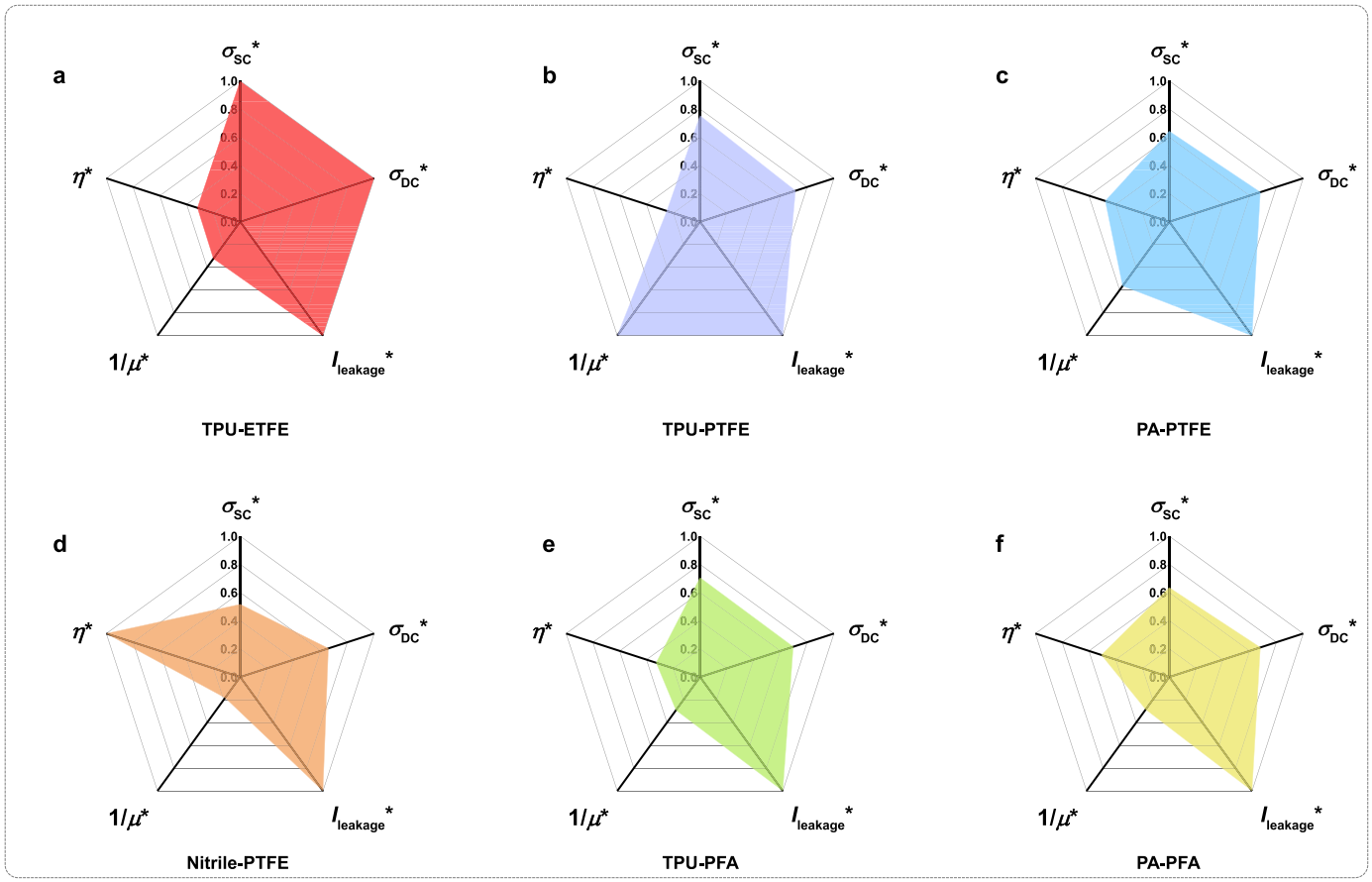

Fig. 4. Comprehensive selection rules of triboelectric material pairs for DEDC-TENG. The radar chart of normalized indexes of TPU-ETFE, TPU-PTFE, PA-PTFE, Nitrile-PTFE, TPU-PFA, PA-PFA where the σ_{SC}* , σ_{DC}* , $I_{leakage}$* , η * , and $1/\mu$ * are the normalization of σ_{SC}, σ_{DC}, $I_{leakage}$, η and $1/\mu$.

which efficiently solved this problem and extended the service life.

2.5. The applications of micro-structured TENGs

To further demonstrate the practical application of TENG with TPU-ETFE as TMP, we design a micro-structured AC-TENG (MAC-TENG) and micro-structured DC-TENG (MDC-TENG), respectively. The 3D schematic illustration of MAC-TENG with TPU-ETFE as the TMP is depicted in Fig. 5a. The structure of the device is composed of two parts, namely the stator and the slider, and the detail fabricated process is exhibited in Experimental Section. As depicted in Fig. S12a-S12c, with the acceleration of sliding changing from 0.1 m s^{-2} to 0.4 m s^{-2}, the transferred charges keep a stable value while the short-circuit current and voltage increase from 5.2 μA to 10.6 μA, from 1578 V to 1962.9 V, respectively. The MAC-TENG working at 0.4 m s^{-2} with a full-wave rectifier can power the capacitors of 1.1 μF, 2.2 μF and 4.7 μF to 5 V only needing 2.6, 4.8, and 10.5 s (Fig. 5b-c), respectively, which demonstrate the good TE performance of the TPU-ETFE pair.

Then, we fabricated a MDC-TENG with TPU-ETFE as the TMP to demonstrate its excellent comprehensive performance (Fig. 5d). The MDC-TENG contains four DC-TENG units. As shown in Fig. S13, the transferred charge of MDC-TENG in one cycle at 0.85 Hz is 649 nC. To boost the energy utilization efficiency, we designed a power management circuit (PMC) consisting of an input capacitor C_{in}, a buck circuit and a mechanical switch (Fig. 5e). The capacitor of 340 pF was selected as the best C_{in} to maximize the energy output [32–34] (Fig. S14). With the help of the PMC, it only took 8.3, 17.7, and 41.4 s to charge the 47, 100, and 220 μF capacitors to 3 V, respectively, by the MDC-TENG working at 0.85 Hz (Fig. S15). By changing the output capacitor (C_{out}) in the buck circuit, the pulse and steady output current can be easily regulated. With the C_{out} of 100 nF, a pulsed current with the peak value of approximate 15 μA was obtained, so 40 LEDs with 10 mm diameter connected in parallel can be powered with instantaneous flashing by the MDC-TENG at 0.85 Hz (Fig. 5f, Fig. S16 and Video S1). With the C_{out} of 470 μF, a stable current of approximate 12 μA was obtained and the hygrothermograph was continuouslly driven by MDC-TENG working at 0.85 Hz with PMC (Fig. 5g-h, Fig. S17 and Video S2). The above applications strongly demonstrate the excellent comprehensive performance of TPU-ETFE as the TMP in both AC-TENG and DC-TENG.

Supplementary material related to this article can be found online at doi:10.1016/j.nanoen.2023.108509.

3. Conclusions

In summary, we provide a universal strategy to assess the suitability of a TMP for DEDC-TENG based on assessing the friction coefficient, surface charge density, leakage current, breakdown density and breakdown efficiency. Based on the analyze of the charge generation and charge transportation processes of DEDC-TENG, we first measured the friction coefficient and triboelectric charge density, and then investigated the leakage current, breakdown density, polarization tensity, and breakdown efficiency in the DEDC-TENG. According to the experimental comparison, a radar chart is established for the TMP selection, and the TPU-ETFE pair presents excellent output performance based on the strategy that we proposed. For demonstration purpose, a MDC-TENG are fabricated to demonstrate the energy conversion ability of ETFE-TPU. The MDC-TENG with four units can be used for powering 40 LEDs or a hygrothermograph at the low working frequency of 0.85 Hz with a designed PMC. This work provides an effective strategy to select appropriate TMPs to optimize the performance of DC-TENG, and

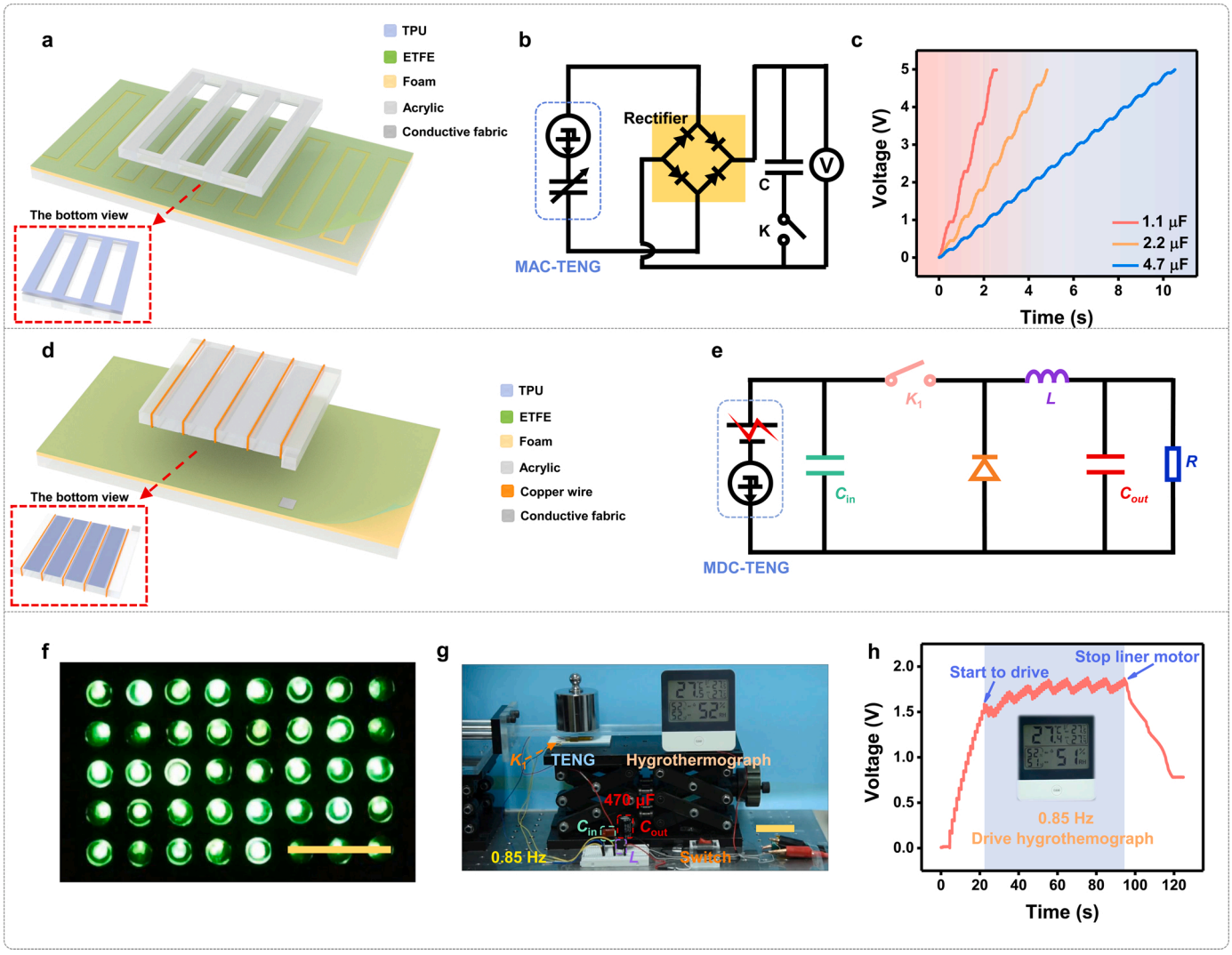

Fig. 5. The output performance and applications of micro-structured TENGs with the TPU-ETFE as TMP. (a) Schematic illustration of MAC-TENG. Inset shows the bottom view of the slider. (b) The circuit diagram of MAC-TENG to charge the capacitor. (c) Charging curves of capacitors with various capacitance by MAC-TENG. (d) Schematic illustration of MDC-TENG. Inset shows the bottom view of the slider. (e) Circuit diagram of the MDC-TENG layer for powering the external load through PMC. Actual image of (f) 40 LEDs and (g) one hygrothermograph driven by the MDC-TENG at 0.85 Hz with PMC. Scale bar, 5 cm. (h) Voltage of the hygrothermograph continually driven by the MDC-TENG working at 0.85 Hz with PMC.

highlights regulating the charge generation and transportation process in DC-TENG to optimize its performance, which is also helpful for understanding the other TENGs.

4. Experimental section

4.1. The measurement of friction coefficient

The device which was measured contained two parts: For the slider, a piece of acrylic sheet with dimensions of 20 × 20 × 5 mm was cut as substrate by a laser cutter. Then, a piece of copper foil with dimensions of 20 × 20 × 0.05 mm was cut and pasted on the substrate. A piece of top dielectric layer (TPU, PA, Nitrile) with dimensions of 20 × 20 mm and pasted on the electrode as triboelectric layer. For the stator, a piece of acrylic sheet with dimensions of 30 × 120 × 5 mm was cut as substrate by a laser cutter. To keep sufficient contact, a piece of foam with dimensions of 30 × 120 mm was cut and pasted on the substrate. At last, a piece of bottom dielectric layer (ETFE, PTFE, PFA, FEP, PVC, PET, PC) with dimensions of 30 × 60 mm was cut and pasted on the electrode as triboelectric layer. One end of the tension gauge was connected to the slider and the other end to the linear motor. As the linear motor moving, the tension meter will show the amount of tension.

4.2. Fabrication of AC-TENG

The freestanding mode AC-TENG consisted of two parts: For the slider, a piece of acrylic sheet with dimensions of 20 × 20 × 5 mm was cut as substrate by a laser cutter. Then, a piece of copper foil with dimensions of 20 × 20 × 0.05 mm was cut and pasted on the substrate as electrode. A piece of top dielectric layer (PA, Nitrile) with dimensions of 20 × 20 mm was cut and pasted on the electrode as triboelectric layer. For the stator, a piece of acrylic sheet with dimensions of 30 × 60 × 5 mm was cut as substrate by a laser cutter. To keep sufficient contact, a piece of foam with dimensions of 30 × 60 mm was cut and pasted on the substrate. Then, two pieces of copper foil with dimensions of 30 × 30 × 0.05 mm was cut and pasted with small gap of 1 mm on the foam as electrodes. At last, a piece of bottom dielectric layer (ETFE, PTFE, PFA, FEP, PVC, PET, PC) with dimensions of 30 × 60 mm was cut and pasted on the electrode as triboelectric layer.

4.3. Fabrication of DC-TENG

The DC-TENG consisted of two parts: For the slider, a piece of acrylic sheet with dimensions of 20 × 20 × 5 mm was cut as substrate by a laser cutter. Then, a piece of copper foil with dimensions of 20 × 20 × 0.05 mm was cut and pasted on the substrate as back electrode. A piece of copper foil with dimensions of 5 × 20 × 0.05 mm was cut and pasted on the right of the acrylic as charge collecting electrode. There was a gap of about 1 mm between the copper foil and the charge collecting electrode. A piece of top dielectric layer with dimensions of 20 × 20 mm and pasted on the black electrode. A gap about 0.5 mm was between the top dielectric layer and charge collecting electrode. For the stator, a piece of acrylic sheet with dimensions of 30 × 60 × 5 mm was cut as substrate by a laser cutter. To keep sufficient contact, a piece of foam with dimensions of 30 × 60 mm was cut and pasted on the substrate. At last, a piece of bottom dielectric layer with dimensions of 30 × 60 mm was cut and pasted on the electrode as triboelectric layer. Note: The thickness of TPU is 10 μm; PA is 10 μm; and Nitrile is 60 μm. The thickness of nitrile is 50 μm thicker than TPU and PA. Therefore, for the slider of device with Nitrile as top dielectric layer, the 5 × 20 × 0.05 mm charge collecting electrode was attached on the same plane as back electrode and kept a gap about 1 mm to the back electrode. When the DC-TENG is driven by linear motor, the contact force is 10 N; the sliding distance is 30 mm; and the acceleration is 0.1 m s^{-2}.

4.4. Fabrication of Micro-structured AC-TENG

Micro-structured AC-TENG with TPU-ETFE layer as TMP contained two parts: For the slider, a piece of grid-acrylic with dimensions of 45 × 41 × 5 mm was cut as substrate by a laser cutter. Then, a piece of conductive fabric with same size was pasted on the substrate as electrode. At last, a piece of TPU with same size was pasted on it as top dielectric layer. For the stator, a piece of acrylic sheet with dimensions of 51 × 95 × 5 mm was cut as substrate by a laser cutter. To keep sufficient contact, a piece of foam with same size was cut and pasted on the substrate. Then, two pieces of conductive fabric with grating segments shape was pasted on it as electrode. At last, a piece of ETFE with dimensions of 51 × 95 mm was cut and pasted on the electrode as triboelectric layer.

4.5. Fabrication of MDC-TENG

MDC-TENG with TPU-ETFE layer as TMP contained two parts: For the slider, a piece of acrylic sheet with dimensions of 30 × 35 × 5 mm was cut as substrate by a laser cutter. Five grooves of equal depth were alternately carved in the middle of the substrate by controlling the laser power and rate. The copper wire was embedded into the grooves as charge collecting electrode. Four pieces of conductive fabrics with size of 30 × 4 × 0.1 mm were attached on the substrate as back electrode and kept a 1 mm gap with charge collecting electrode. Then four pieces of TPU with size of 30 × 5 × 0.01 mm were attached on the conductive fabrics and kept a 0.5 mm gap with charge collecting electrode. At last, a piece of acrylic sheet with dimensions of 40 × 45 × 5 mm was cut as substrate by a laser cutter. And the above device was attached on it. For the stator, a piece of acrylic sheet with dimensions of 30 × 60 × 5 mm was cut as substrate by a laser cutter. To keep sufficient contact, a piece of foam with dimensions of 30 × 60 mm was cut and pasted on the substrate. At last, a piece of friction layer with dimensions of 30 × 60 mm was cut and pasted on the electrode as triboelectric layer.

4.6. Characterization and electrical measurement

The sliding process was driven by a linear motor (TSMV120–1S). The acceleration of sliding is 0.1 m s^{-2} and the force is 10 N. The short-circuit current, voltage, and transferred charges of the TENG were measured by a programmable electrometer (Keithley model 6514). The leakage current of dielectric layer was measured by the High Precision Insulation Resistance Meter (TH2684A).

CRediT authorship contribution statement

Shengnan Cui: Conceptualization, Methodology, Data curation, Investigation, Writing - original draft, Writing - review & editing. **Di Liu**: Conceptualization, Methodology, Investigation, Writing - review & editing. **Peiyuan Yang**: Methodology. **Jiaqi Liu**: Methodology. **Yikui Gao**: Investigation. **Zhihao Zhao:** Methodology. **Linglin Zhou**: Methodology. **Jiayue Zhang**: Methodology. **Wang Zhonglin**: Supervision, Writing – review & editing. **Jie Wang**: Supervision, Conceptualization, Writing – review & editing.

Declaration of Competing Interest

The authors declare that they have no known competing financial interests or personal relationships that could have appeared to influence the work reported in this paper.

Data availability

Data will be made available on request.

Acknowledgments

Research was supported by the National Key R & D Project from Minister of Science and Technology (2021YFA1201602), National Natural Science Foundation of China (Grant No. U21A20147, 62204017 and 22109013), China Postdoctoral Science Foundation (2021M703172), Innovation Project of Ocean Science and Technology (22–3-3-hygg-18-hy), the Fundamental Research Funds for the Central Universities (E1E46802) and the National Key R & D Project from Minister of Science and Technology (2021YFA1201602).

Appendix A. Supporting information

Supplementary data associated with this article can be found in the online version at doi:10.1016/j.nanoen.2023.108509.

References

[1] Z.L. Wang, Entropy theory of distributed energy for internet of things, Nano Energy 58 (2019) 669–672.
[2] F.-R. Fan, Z.-Q. Tian, Z. Lin Wang, Flexible triboelectric generator, Nano Energy 1 (2012) 328–334.
[3] Z.L. Wang, Triboelectric nanogenerators as new energy technology and self-powered sensors – principles, problems and perspectives, Faraday Discuss. 176 (2014) 447–458.
[4] L. Zhou, D. Liu, J. Wang, Z.L. Wang, Triboelectric nanogenerators: fundamental physics and potential applications, Friction 8 (2020) 481–506.
[5] T. Cheng, Q. Gao, Z.L. Wang, The current development and future outlook of triboelectric nanogenerators: a survey of literature, Adv. Mater. Technol. 4 (2019), 1800588.
[6] Z.L. Wang, J. Chen, L. Lin, Progress in triboelectric nanogenerators as a new energy technology and self-powered sensors, Energy Environ. Sci. 8 (2015) 2250–2282.
[7] Z.L. Wang, On the first principle theory of nanogenerators from maxwell's equations, Nano Energy 68 (2020), 104272.
[8] C. Wu, A.C. Wang, W. Ding, H. Guo, Z.L. Wang, Triboelectric nanogenerator: a foundation of the energy for the new era, Adv. Energy Mater. 9 (2019), 1802906.
[9] S. Niu, Y. Liu, S. Wang, L. Lin, Y.S. Zhou, Y. Hu, Z.L. Wang, Theory of sliding-mode triboelectric nanogenerators, Adv. Mater. 25 (2013) 6184–6193.
[10] J. Peng, S.D. Kang, G.J. Snyder, optimization principles and the figure of merit for triboelectric generators, Sci. Adv. 3 (2017), eaap8576.
[11] C. Jiang, K. Dai, F. Yi, Y. Han, X. Wang, Z. You, Optimization of triboelectric nanogenerator load characteristics considering the air breakdown effect, Nano Energy 53 (2018) 706–715.
[12] S. Wang, Y. Xie, S. Niu, L. Lin, C. Liu, Y.S. Zhou, Z.L. Wang, Maximum surface charge density for triboelectric nanogenerators achieved by ionized-air injection: methodology and theoretical understanding, Adv. Mater. 26 (2014) 6720–6728.
[13] H. Zou, Y. Zhang, L. Guo, P. Wang, X. He, G. Dai, H. Zheng, C. Chen, A.C. Wang, C. Xu, Z.L. Wang, Quantifying the triboelectric series, Nat. Commun. 10 (2019) 1427.

[14] J. Wang, S. Li, F. Yi, Y. Zi, J. Lin, X. Wang, Y. Xu, Z.L. Wang, Sustainably powering wearable electronics solely by biomechanical energy, Nat. Commun. 7 (2016), 12744.
[15] J. Wang, C. Wu, Y. Dai, Z. Zhao, A. Wang, T. Zhang, Z.L. Wang, Achieving ultrahigh triboelectric charge density for efficient energy harvesting, Nat. Commun. 8 (2017) 88.
[16] D. Liu, X. Yin, H. Guo, L. Zhou, X. Li, C. Zhang, J. Wang, Z.L. Wang, A constant current triboelectric nanogenerator arising from electrostatic breakdown, Sci. Adv. 5 (2019), eaav6437.
[17] D. Liu, L. Zhou, Z.L. Wang, J. Wang, Triboelectric nanogenerator: from alternating current to direct current, iScience 24 (2021), 102018.
[18] Z. Zhao, Y. Dai, D. Liu, L. Zhou, S. Li, Z.L. Wang, J. Wang, Rationally patterned electrode of direct-current triboelectric nanogenerators for ultrahigh effective surface charge density, Nat. Commun. 11 (2020) 6186.
[19] L. Zhou, D. Liu, Z. Zhao, S. Li, Y. Liu, L. Liu, Y. Gao, Z.L. Wang, J. Wang, Simultaneously enhancing power density and durability of sliding-mode triboelectric nanogenerator via interface liquid lubrication, Adv. Energy Mater. 10 (2020), 2002920.
[20] Z. Zhao, L. Zhou, S. Li, D. Liu, Y. Li, Y. Gao, Y. Liu, Y. Dai, J. Wang, Z.L. Wang, Selection rules of triboelectric materials for direct-current triboelectric nanogenerator, Nat. Commun. 12 (2021) 4686.
[21] D. Liu, L. Zhou, S. Li, Z. Zhao, X. Yin, Z. Yi, C. Zhang, X. Li, J. Wang, Z.L. Wang, Hugely enhanced output power of direct-current triboelectric nanogenerators by using electrostatic breakdown effect, Adv. Mater. Technol. 5 (2020), 2000289.
[22] Z. Yi, D. Liu, L. Zhou, S. Li, Z. Zhao, X. Li, Z.L. Wang, J. Wang, Enhancing output performance of direct-current triboelectric nanogenerator under controlled atmosphere, Nano Energy 84 (2021), 105864.
[23] S. Chen, D. Liu, L. Zhou, S. Li, Z. Zhao, S. Cui, Y. Gao, Y. Li, Z.L. Wang, J. Wang, Improved output performance of direct-current triboelectric nanogenerator through field enhancing breakdown effect, Adv. Mater. Technol. 6 (2021), 2100195.
[24] Z. Zhao, D. Liu, Y. Li, Z.L. Wang, J. Wang, Direct-current triboelectric nanogenerator based on electrostatic breakdown effect, Nano Energy 102 (2022), 107745.
[25] D. Liu, L. Zhou, S. Cui, Y. Gao, S. Li, Z. Zhao, Z. Yi, H. Zou, Y. Fan, J. Wang, Z. L. Wang, Standardized measurement of dielectric materials' intrinsic triboelectric charge density through the suppression of air breakdown, Nat. Commun. 13 (2022) 6019.
[26] W. He, W. Liu, J. Chen, Z. Wang, Y. Liu, X. Pu, H. Yang, Q. Tang, H. Yang, H. Guo, C. Hu, Boosting output performance of sliding mode triboelectric nanogenerator by charge space-accumulation effect, Nat. Commun. 11 (2020) 4277.
[27] Y. Du, S. Fu, C. Shan, H. Wu, W. He, J. Wang, H. Guo, G. Li, Z. Wang, C. Hu, A novel design based on mechanical time-delay switch and charge space accumulation for high output performance direct-current triboelectric nanogenerator, Adv. Funct. Mater. 32 (2022), 2208783.
[28] S. Cui, L. Zhou, D. Liu, S. Li, L. Liu, S. Chen, Z. Zhao, W. Yuan, Z.L. Wang, J. Wang, Improving performance of triboelectric nanogenerators by dielectric enhancement effect, Matter 5 (2022) 180–193.
[29] Z.L. Wang, From contact electrification to triboelectric nanogenerators, Rep. Prog. Phys. 84 (2021), 096502.
[30] Z.L. Wang, A.C. Wang, On the origin of contact-electrification, Mater. Today 30 (2019) 34–51.
[31] X. Qu, Z. Liu, P. Tan, C. Wang, Y. Liu, H. Feng, D. Luo, Z. Li, Z.L. Wang, Artificial tactile perception smart finger for material, Sci. Adv. 8 (2022), eabq2521.
[32] Z. Cao, Z. Wu, R. Ding, S. Wang, Y. Chu, J. Xu, J. Teng, X. Ye, A compact triboelectric nanogenerator with ultrahigh output energy density of 177.8 J m^{-3} via retarding air breakdown. Nano Energy 93 (2022), 106891.
[33] W. Harmon, H. Guo, D. Bamgboje, T. Hu, Z.L. Wang, Timing strategy for boosting energy extraction from triboelectric nanogenerators, Nano Energy 85 (2021), 105956.
[34] Y. Gao, D. Liu, Y. Li, J. Liu, L. Zhou, X. Li, Z. Zhao, S. Li, P. Yang, Z.L. Wang, J. Wang, Achieving high-efficient triboelectric nanogenerators by suppressing electrostatic breakdown effect, Energy Environ. Sci. (2023), https://doi.org/10.1039/D3EE00220A.

Shengnan Cui received her B.S. degree from Qingdao University of Science and Technology. Currently, she is pursuing her Ph.D. degree at Beijing Institute of Nanoenergy and Nanosystems, Chinese Academy of Sciences. Her research interests focus on performance improvement of triboelectric nanogenerators.

Dr. Di Liu received his B. S. degree in Material Science and Engineering from Nanjing University of Aeronautics and Astronautics, China. Then, he received his Ph.D. degree in Materials Science from University of Chinese Academy of Sciences, China. Now, he is a postdoctoral fellow in Beijing Institute of Nanoenergy and Nanosystems, Chinese Academy of Sciences. His current research interests focus on triboelectric nanogenerators, electrostatic breakdown and self-powered systems.

Peiyuan Yang received his B. S. degree in Physics from Nanjing University of Information Science and Technology. Currently, he is pursuing his master's degree in Guangxi University. His current research interest is bule energy and charge pump system of triboelectric nanogenerators.

Jiaqi Liu received her B. S. degree in Physics from Jilin University. Currently, she is pursuing her master's degree in Guangxi University. Her current research interest is performance improvement of triboelectric nanogenerators.

Yikui Gao received his B. S. degree in Theoretical physics from Chongqing University. Currently, he is pursuing his Ph.D. in Beijing Institute of Nanoenergy and Nanosystems, Chinese Academy of Sciences, China. His current research interest is triboelectric nanogenerator.

Dr. Zhihao Zhao received the Ph.D. degree in Materials Science and Engineering from Tianjin University in 2018. After graduation, he worked as a postdoctoral research fellow in School of Materials of Sun Yat-sen University. Currently, he is an associate professor of Beijing Institute of Nanoenergy and Nanosystems. His current research interests focus on triboelectric nanogenerators, and dielectric/piezoelectric materials.

Dr. Linglin Zhou received her Ph.D. degree from University of Science and Technology of China in 2018. Now she is a research assistant in Beijing Institute of Nanoenergy and Nanosystems, Chinese Academy of Sciences, China. Her current research focuses on the improvement of triboelectric nanogenerators and their applications in environmental pollutants treatment.

Jiayue Zhang received her B.S. degrees from Chongqing University and University of Cincinnati in Mechanical Engineering. Now she is a Ph.D. candidate in Tsinghua University, China. Her current research interest is nanogenerators and self-powered systems.

Prof. Zhong Lin (ZL) Wang received his Ph.D. from Arizona State University in physics. He now is the Hightower Chair in Materials Science and Engineering, Regents' Professor, Engineering Distinguished Professor and Director, Center for Nanostructure Characterization, at Georgia Tech. Dr. Wang has made original and innovative contributions to the synthesis, discovery, characterization and understanding of fundamental physical properties of oxide nanobelts and nanowires, as well as applications of nanowires in energy sciences, electronics, optoelectronics and biological science. His discovery and breakthroughs in developing nanogenerators established the principle and technological road map for harvesting mechanical energy from environment and biological systems for powering a personal electronics. His research on self-powered nanosystems has inspired the worldwide effort in academia and industry for studying energy for micro-nano-systems, which is now a distinct disciplinary in energy research and future sensor networks. He coined and pioneered the field of piezotronics and piezo-phototronics by introducing piezoelectric potential gated charge transport process in fabricating new electronic and optoelectronic devices. Details can be found at: http://www. nanoscience.gatech.edu.

Prof. Jie Wang received his Ph.D. degree from Xi'an Jiaotong University in 2008. He is currently a professor at Beijing Institute of Nanoenergy and Nanosystems, Chinese Academy of Sciences. His current research interests focus on the energy materials, supercapacitors, nanogenerators and self-powered system.